Winter 12-2013

Experimental study on the effect of air flow on soap bubble formation

John M. Davidson
University of Nebraska at Lincoln, jdav.nexus@gmail.com

EXPERIMENTAL STUDY ON THE EFFECT OF AIR FLOW ON SOAP BUBBLE FORMATION

by

John M. Davidson

A THESIS

Presented to the Faculty of

The Graduate College at the University of Nebraska

In Partial Fulfillment of Requirements

For the Degree of Master of Science

Major: Mechanical Engineering and Applied Mechanics

Under the Supervision of Professor Sangjin Ryu

Lincoln, Nebraska

December 2013

EXPERIMENTAL STUDY ON THE EFFECT OF AIR FLOW ON SOAP BUBBLE FORMATION

John Michael Davidson, M.S.

University of Nebraska, 2013

Advisor: Sangjin Ryu

Soap bubbles are a common interfacial fluid dynamics phenomenon having applications such as buoyant hollow spherical fillers and flow visualization of large scale airflows. In contrast to the dynamics of liquid drops in gas and gas bubbles in liquid, the dynamics of soap bubbles has not been well documented, possibly because soap bubbles have gas-liquid-gas interfaces. Having the thin-liquid-film interface seems to alter the characteristics of the bubble/drop creation process. Thus, the main objective of this study is to experimentally examine how airflow develops and interacts with the soap liquid film as the film stretches and finally collapses to pinch-off.

A soap bubble blowing apparatus was constructed to consistently reproduce soap bubble blowing process with various soap ring sizes, and high-speed videography was utilized to investigate the blowing process. The minimum radius of the neck of the soap liquid tube was measured when approaching pinch-off. It is seen that the minimum neck radius is approximately proportional to the time left till pinch-off by a scaling exponent of about 2/3. The exponent is 1/3 for a gas bubble in liquid and 2/3 for a liquid drop in gas. This indicates that liquid drops collapse more slowly than gas bubbles because the liquid is more viscous and that soap bubbles show slower collapses due to two gas-liquid interfaces.

One observed difference in soap bubble pinch-off due to the different ring size was that the pinch-off process followed the scaling law less as the ring became smaller.

Based on this observation, a hypothesis was proposed that airflow outside the soap liquid tube causes variances in the pinch-off of the tube. To test the hypothesis, particle image velocimetry was used to observe the effects of airflow on the growing soap liquid tube. It is shown that the smaller rings more interfere with the airflow causing perturbation and thus increase the deviation from the scaling law, which supports our hypothesis.

Contents

List of Figures

Chapter 1

Introduction

Soap bubbles are a common inter-facial fluid dynamics phenomenon that has fascinated people, from children to artists and scientist for centuries [1–3]. However, there has not been much research performed to determine the scaling law or the effect they have on airflow when forming. Similar topics like liquid droplets in gas and gas bubbles in liquid have been extensively studied, but the behavior of the gas-liquid-gas of soap bubbles on the formation has not been deeply analyzed. This is partly due to the fact that liquid droplets and gas bubbles are phenomenons that have a large effect on industry. Gas bubble formation have a large effect in medical applications and both droplets have a huge impact on ink-jet technology [4–6]. Furthermore, as microfluidics become more popular, micro-bubble and droplet formation in flow-focusing devices have seen an increase in study [5, 7].

This is not to say that soap bubble formation is unimportant. One application of liquid-film bubbles is micro-spheres made from glass, ceramics, or polymers which add compressive strength to solid compounds while reducing the weight. Microspheres have impact in light weight concrete, ships and submersion devices that need to withstand high pressure, as well as reducing the weight of an aircraft without compromising their integrity [8, 9]. A possible application of soap bubbles is being

considered in the study of turbines. Wind turbines have been reported to cause fatalities to birds and bats that are possibly affected by the high pressure fluctuation caused by moving wind turbine blades [10]. It is important to measure the pressures around turbines to determine whether the pressure is in fact an issue. More traditional methods, such as pressure taps, pitot tubes, and drones with pressure sensors, are not feasible due to the cost and interference they would have on the system. One possibility is to introduce soap bubbles of different volumes into the flow and record when they burst. The size of the bubbles will determine at what pressure they will rupture, thus it is important to determine how to affectively control the bubble's size. Also, the bubbles will help to trace the flow; since the bubbles are of the same gas as the fluid, the buoyancy or gravitational effects are negligible and the resultant flow should be accurate.

For such applications, this research attempts to determine what factors influence the soap bubble when forming. The pinch-off will be examined to see the trends and governing laws that control the soap bubble's formation. Furthermore, particle image velocimetry (PIV) will be used to analyze the affect the flow has on bubble formation.

Chapter 2

Background

In order to understand the results, it is important to first understand the governing concepts that may control the size of the soap bubbles. To begin, the structure of the soap film will be discussed. Next, three concepts that control soap bubbles and soap films will be described: surface tension, the Young-Laplace equation, and free energy. Also, a phenomenon known as the Plateau-Rayleigh instability will be examined because it may effect the growing soap film and how repeatable the formation of the soap bubble is. A further issue may also arise from the Marangoni and gravitational forces that keep a bubble in equilibrium but also cause the bubble to have a varying thickness. After these topics are discussed, previous findings on the pinch-off of gas bubbles and droplets will be discussed for a comparison between gas-liquid interface and gas-liquid-gas interface systems.

2.1 Soap Film Structure

Soap bubbles and soap films are possible due to the unique molecular interactions occurring at the surface of the soap solution. A soap solution is comprised of two parts: a liquid and a surfactant that forms a layer at the surface of the liquid. The surfactant is an amphipathic ion that has a hydrophilic head that tries to remain

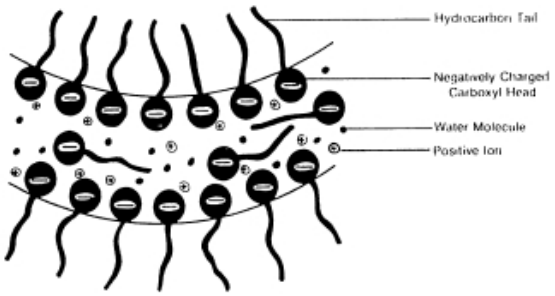

Figure 2.1: The molecular structure of the film [11]

surrounded by water and a hydrophobic tail that repels from the water molecules (see Fig. 2.1) [11]. The hydrophobic tail causes the surfactant molecules to settle at gas-liquid interface [11].

A usual soap particle the head is a polar carboxyl and the tail is a hydrocarbon chain. Sodium stearate ($C_{17}H_{35}COO^{-}Na^{+}$) is one example. The hydrophilic polar carboxyl head is COO^{-}, the hydrophobic hydrocarbon tail is $C_{17}H_{35}$, and Na^{+} is an accompanying positive ion [11]. The ideal arrangement for these two-part molecules is the surface of the liquid where the head can be surrounded by water molecules while the tail can protrude from the surface and avoid any water molecules (Fig. 2.1). In the case of a soap film, there are two surfaces and the amphipathic molecules can disperse across both surfaces.

2.2 Surface Tension

The main fluid property that governs soap films is the surface tension of the soap liquid. Surface tension arises from the molecular attraction along an interface between two media (Fig. 2.2). The coefficient of surface tension describes the energy required to increase surface area [11]. The molecules in the bulk of the fluid experience forces equally in all directions from the surrounding molecules. In contrast, the molecules along the surface have a larger force acting on it from other liquid molecules than

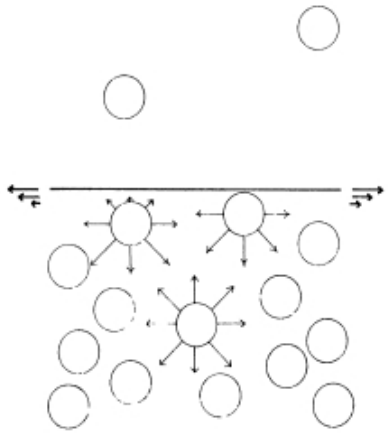

Figure 2.2: Intermolecular forces on liquid molecules in the bulk and at the surface of the fluid [11]

.

from bordering gas molecules. The resulting interacting forces between the liquid molecules in comparison to the weaker forces between the gas and liquid molecules creates the surface tension along the interface. Because of the way the molecules act on each other, the surface tension can also be described as a force per length acting parallel to the interface and normal to the boundary. When applied to a soap film, the film will be under constant tension due to the surface tension. In fact, the force is proportional to twice the surface tension due to the existence of two interfaces. This constant tension will try to minimize the area of the soap film as will be discussed in Section 2.3.

As explained in Section 2.1, soap solutions contain not only the liquid molecules but also the soap molecules. Each soap molecule has a hydrocarbon tail that tries to break through the surface due to its hydrophobic nature (Fig. 2.3a). This interferes with the attraction forces between the liquid molecules lining the surface of the solution, reducing the surface tension [11]. Therefore, the surface tension decreases as the concentration of the soap molecules increases until it reaches the minimum surface tension when no further soap molecule can break the surface (Fig. 2.3b). The minimum surface tension depends on the surfactant but is usually one-third of the

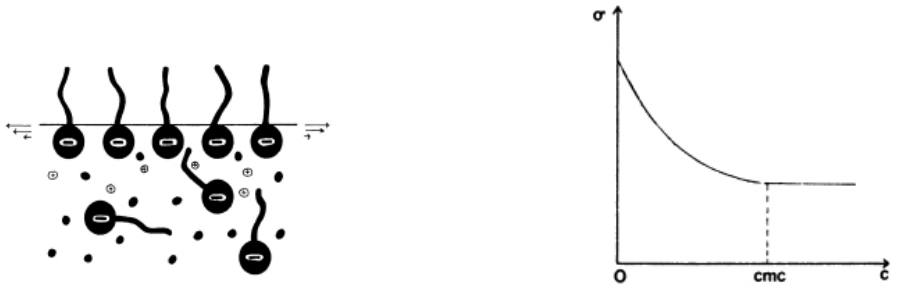

(a) (b)

Figure 2.3: The effect of soap molecules on the surface tension of a solution. (a) depicts how the soap molecules interfere with the liquid molecules along the surface. (b) shows the surface tension, σ, versus the concentration of the soap molecules, c. [11]

pure liquid surface tension [11].

2.3 Free Energy

The second attribute of soap films to be considered is the free energy of the film. The surface area of the soap bubble is limited by the energy of the film. Using surface tension, the energy of a small segment of soap film is given by

$$\sigma dxdy = \sigma dA \tag{2.1}$$

where dA is the area of the segment. The total energy of the bubble or film is given by integrating over the entire area:

$$F = \int_0^A \sigma dA \tag{2.2}$$

where F is the free energy required to increase the area from zero to the entire area of the film. In a soap solution, the surface tension is dependent on the concentration of the surfactant in the liquid, commonly water. However, if the concentration of the surfactant is assumed large, the surface tension can be assumed constant and the free

energy becomes

$$F = \sigma A. \tag{2.3}$$

Therefore, the energy of the soap film is directly proportional to the area [11].

The surface tension tries to minimize the free energy. Therefore the surface area will be reduced as much as possible. For a completed soap bubble, this means that the soap bubble would be a sphere [11]. For growing soap bubbles, the surface tension tries to keep the film as small as possible while the jet fights to increase the size of the film. Eventually, it will grow too large and the soap film will pinch-off to maintain a minimal surface area.

2.4 The Young-Laplace Equation

The next aspect of soap films and bubbles that will be considered is the Young-Laplace equation. The Young-Laplace equation describes the pressure difference across an interface as a function of the surface tension and the radius of the interface's curvature and is written as

$$\Delta p = \sigma \left(\frac{1}{R_1} + \frac{1}{R_2} \right) \tag{2.4}$$

where Δp is the pressure difference, σ is the surface tension, and R_1 and R_2 are the two principle curvature radii of the interface. For a sphere, the two principle radii are equal and the Young-Laplace equation becomes

$$\Delta p = \sigma \frac{2}{R} \tag{2.5}$$

This relationship implies that as the radius of the sphere decreases, the pressure increases. A smaller sphere or bubble will have a greater pressure than a larger sphere or bubble.

One further step is needed for soap films and bubbles. In the case of two gas-liquid

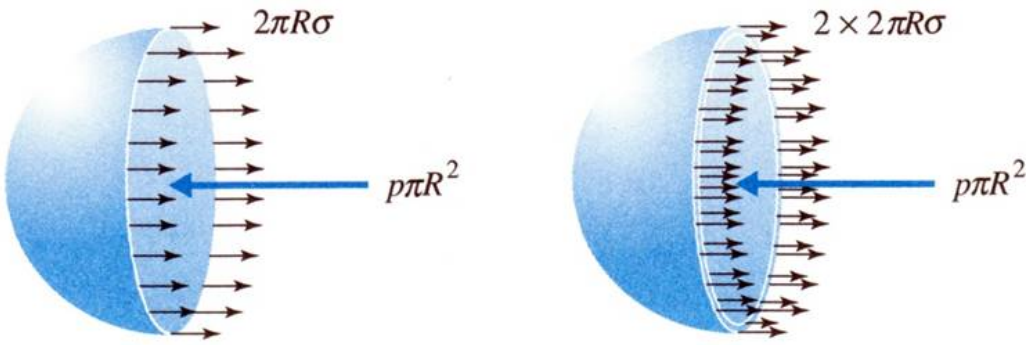

Figure 2.4: The differences between the single and the two gas-liquid interface [12]

interfaces, the pressure difference across both surfaces needs to be considered. These differences can be added and Eq. 2.5 becomes:

$$\Delta p = \Delta p_1 + \Delta p_2 = \sigma \frac{2}{R} + \sigma \frac{2}{R} = \frac{4\sigma}{R} \tag{2.6}$$

Fig. 2.4 shows the difference between the single interface system and the two gas-liquid interface system.

2.5 Plateau-Rayleigh Instability

A phenomenon worth observing is the Plateau-Rayleigh Instability of cylindrical columns of fluid. Consider a stream of water flowing from a faucet. It is common that the stream of water will break up into drops. This is because drops have a smaller surface area than the column of water and thus they have less free energy [13]. This can be shown through the comparison of the volume between the drops and the initial column of liquid. If there is n drops of radius r that are produced from the column of liquid with radius R and length L, the conservation of volume would look like

$$\pi R^2 L = \frac{4}{3}\pi r^3 n. \tag{2.7}$$

The number of droplets with radius r can therefore be shown to be

$$n = \frac{3}{4}\frac{R^2 L}{r^3}. \tag{2.8}$$

When the surface areas of the n droplets, S_n is compared to the surface area of the column, S_0, combined with Eq. 2.8, the ratio is found to be

$$\frac{S_n}{S_0} = \frac{4\pi n r^2}{2\pi R L} = \frac{3}{2}\frac{R}{r}. \tag{2.9}$$

This means that the surface are of n droplets produced from a column of liquid will have less surface area than the original column if $r > \frac{3}{2}R$ [13].

This process was first understood by Plateau, who realized that the cylinder will spontaneously distort itself to minimize its free energy as soon as the wavelength of the distortion, λ_d, is greater than the cylinder's perimeter [13, 14]. This distortion waveform will then amplify until the column breaks into drops of approximately equal size. Lord Rayleigh later showed that the droplet size is determined by the fastest distortion mode [13].

In the case of a jet creating a soap film tube, there exist two separate columns of liquid: the annulus of soap solution and the air trapped inside. It is unclear whether this will have a compound effect and the Plateau-Rayleigh instability will dominate the bubble formation or not.

2.6 Marangoni and Gravitational Forces

One issue that affects soap bubbles and films is the gravitational force. This causes the liquid to flow towards the bottom of the bubble or film, i.e., 'draining' the liquid and threatening the integrity of the structure. Furthermore, it causes a gradient in surface tension due to a lower concentration of soap molecules at the top [15]. At

this point, the Marangoni forces begin to have an effect. The Marangoni forces are due to a variance of surface tension that arises from temperature variations or from inhomogeneous material properties such as the concentration of surfactant. This difference in surface tension causes the molecules to flow towards the higher surface tension area, i.e. the top of the bubble or film. The Marangoni and gravitational forces act on soap bubbles in a constant struggle that in the end balance out to form a stable structure [15].

The existence of this variation in surface properties raises issues that cannot be avoided. When considering the surface tension of the soap film, the surface tension of the soap solution will be considered. This surface tension in reality will be an average of the surface tension of the film. The gradient of the surface tension combined with the increased film thickness at the bottom may cause asymmetry in the formation of the bubble. This Asymmetry could accelerate existing instabilities such as the Plateau-Rayleigh instability. It can also cause the film to burst prior to pinch-off.

2.7 Property Influences on Gas Bubbles in Liquid

Studies have been performed on the effect of viscosity, surface tension, and density on gas bubbles in liquid. One influential paper is of Ramakrishnan *et al.* [16] who did an experimental study of gas bubble formation in a bath of liquid with constant flow rate. Ramakrishnan *et al.* studied the effects of surface tension and viscosity on the size of the gas bubble.

Ramakrishnan *et al.* [16] found that at low flow rates, the bubble volume greatly depends on the balance of buoyancy and surface tension forces. As the flow rate increases, the change in surface tension has a smaller effect on the bubble size. At high flow rates the surface tension effect becomes negligible. The point at which the surface tension becomes negligible decreases as the viscosity increases.

When observing the influence of viscosity, Ramakrishnan *et al.* [16] determined that an increase in viscosity results in an increase in bubble size. Viscosity also has a large impact when the flow rate is high or the surface tension is low.

2.8 Pinch-off

Another aspect that has been studied on gas bubbles and droplets but not soap bubbles is the pinch-off. As the droplet or bubble forms, the neck of the structure becomes narrower and eventually pinch-off occurs. There have been many studies relating the smallest radius of the neck to the time remaining until pinch-off. This relationship takes the form of the power law dependence

$$r \propto \tau^{\alpha} \tag{2.10}$$

where r is the minimal radius of the neck and τ is the time left to pinch-off [5].

There have been many reports for the value of the power law exponent, α. For a gaseous thread in water, α was calculated to be $1/2$ using a purely liquid inertia driven model [5, 17]. However, α has been shown experimentally to be slightly larger than $1/2$ [5,18]. If a slender-body calculation is performed, α is shown to be dependent on τ in the form of:

$$\alpha(\tau) = 1/2 + (-16\ln(\tau))^{-1/2} \tag{2.11}$$

and α asymptotes to $1/2$ at pinch-off [5]. For a droplet in gas, the power law exponent is described by the balance between surface tension and inertia, and is about $2/3$ (Fig. 2.5) [17, 26]. For a gaseous thread, it was found by Gordillo *et al.* [19] that the gas inertia causes Bernoulli suction and accelerates the pinch-off. Gordillo *et al.* found that α is about $1/3$ (Fig. 2.6) [5, 19].

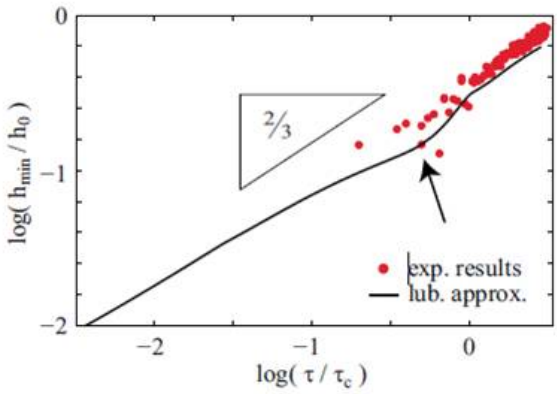

Figure 2.5: Scaling law exponent for a droplet in gas [26].

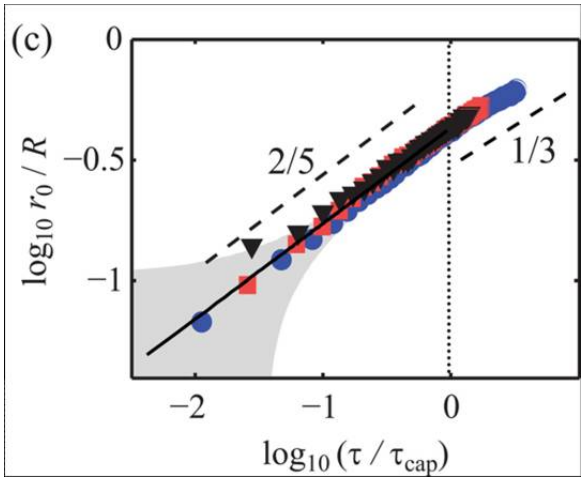

Figure 2.6: Scaling law exponent for a gas bubble in liquid [5]

Chapter 3

Methodology

In order to analyze the bubble formation, it is important to first address two aspects: the jet apparatus and the soap solution. The jet apparatus design will be addressed first and will consist of a pressured air source, a seeding chamber, meshes to control turbulence, and soap rings.

3.1 Design of Jet Apparatus

Before designing the jet apparatus, a few preliminary values are needed. These values are the jet nozzle diameter, the volumetric flow rate through the nozzle, and the pressure difference required to create the flow. The general layout of the apparatus is a Hagen-Poiseuille flow through a pipe to simulate lungs and trachea with a nozzle at the end to simulate the lips. The flow will pass through a series of meshes to stabilize the flow and constrict any rotational flow that may occur in the pipe due to roughness.

3.1.1 Determining Outlet Diameter

Using a high-speed camera (Miro 310, Vision Research), videos of humans blowing soap bubbles were captured. These videos were analyzed and, using a reference height, the diameter of a human's lips when blowing bubbles is determined to be about 4.75 mm. Since this is a non-standard size for commercial pipes, an outlet inner diameter of 6.35 mm (1/4 in) was selected for apparatus simplicity.

3.1.2 Determining Required Flow Velocity

The videos of humans blowing soap bubbles were further analyzed to determine the flow velocity produced by the human. The radii of the bubbles produced by the human were measured as well as the time required for the bubbles to form. The images for radius measurements were selected such that the bubbles were as round as possible and the bubbles were assumed to be spheres at that point. The volumetric flow rate was then calculated using

$$Q = \frac{V_{bubble}}{t} = \frac{\frac{4}{3}\pi r^3}{t} \tag{3.1}$$

where Q is the volumetric flow rate, V_{bubble} is the volume of the bubble, r is the radius of the bubble, and t is the time the bubble takes to form. The volumetric flow rate was calculated to be 412±40 cm^3/s. Although this is a large deviation, the value of 410 cm^3/s was used as an initial value for design.

3.1.3 Determining Required Pressure

Once the volumetric flow rate was determined, the required pressure to produce the flow was calculated. The geometry used for calculation purposes was a 25.4 mm inner diameter pipe flowing through four meshes of mesh size 200, 40, 20, and 10 mesh per inch before passing through a nozzle that reduces the diameter to 6.35 mm

Table 3.1: Values for mesh sizes, wire diameter, solidity, and Reynolds number. $f(\mathrm{Re}_d)$ is based on data collected byJohan Groth and Arne V. Johansson [21] and Δp is the calculated pressure drop.

Mesh Size	Wire Diameter (mm)	Solidity	Re_d	$f(\mathrm{Re}_d)$	Δp (Pa)
200	0.0533	0.66	2.877	3.25	9.77
40	0.254	0.64	13.702	1.50	3.96
20	0.4064	0.54	21.922	1.25	1.83
10	0.635	0.44	34.254	1.00	0.86

inner diameter. A 25.4 mm inner diameter pipe was used since it is a standard pipe diameter and the trachea of a healthy human being has been measured to be in the range of 25.4 mm [20]. Using the average flow velocity of 410 cm^3/s, the average velocity in the pipe was calculated to be 0.809 m/s. Using this velocity and the properties of each mesh, the Reynolds Number and pressure drop for each mesh were calculated and shown in Table 1.

The pressure drop, Δp, is given by

$$K \equiv \frac{\Delta p_{stat}}{\frac{1}{2}\rho U^2} = f(\mathrm{Re}_d)\frac{1-(1-\gamma)^2}{(1-\gamma)^2}, \tag{3.2}$$

where K is the pressure drop coefficient, ρ is the fluid density, $f(\mathrm{Re}_d)$ is a correction factor based on the Reynolds number, and γ is the solidity. The total pressure drop through the four meshes is 16.41 Pa (0.00238 psig). Later it was found that the 200 mesh becomes clogged with impurities in the gas flow and was removed.

Next, the pressure drop through the nozzle was considered. Using Bernoulli's Equation along a streamline

$$\frac{p}{\rho} + \frac{U^2}{2} + gz = Constant. \tag{3.3}$$

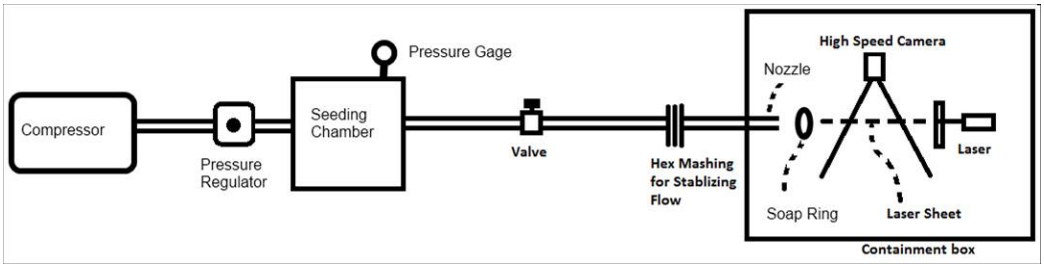

Figure 3.1: Schematic of the jet apparatus.

Given that the volumetric flow rate is

$$Q = UA = U\frac{\pi d^2}{4}, \tag{3.4}$$

and assuming the nozzle is horizontal ($z_1 = z_2$) it can be shown that the pressure drop across a nozzle is

$$\Delta p = \frac{8\rho Q^2}{\pi^2}\left(\frac{1}{d_2^4} - \frac{1}{d_1^4}\right), \tag{3.5}$$

where d_1 is the diameter of the pipe prior to the nozzle and d_2 is the diameter after the nozzle. Using the assumed geometry of $d_1 = 25.4$ mm and $d_2 = 6.35$ mm, the pressure drop was calculated to be 100.17 Pa.

The last pressure drop to be considered was the pressure drop at the nozzle outlet. This was found by using Eq. 3.5 with $d_1 = 1/4$ inch and $d_2 = \infty$. The pressure was calculated to be 100.56 Pa. The total pressure drop, and required pressure in the tank, is therefore 217.14 Pa or 0.0315 psig (about 0.87 in H_2O). Due to pressure gage accuracy concerns, 0.9 in H_2O was used to drive the flow.

3.1.4 Jet Apparatus

Figures 3.1 and 4.5 show the schematics of the jet apparatus and the constructed jet apparatus, respectively. The pressure for the jet will be supplied by an air compressor (150 PSI C2002 compressor, Porter-Cable). The pressure tank will fill a seeding chamber to the appropriate pressure (0.9 in H_2O). The seeding chamber was con-

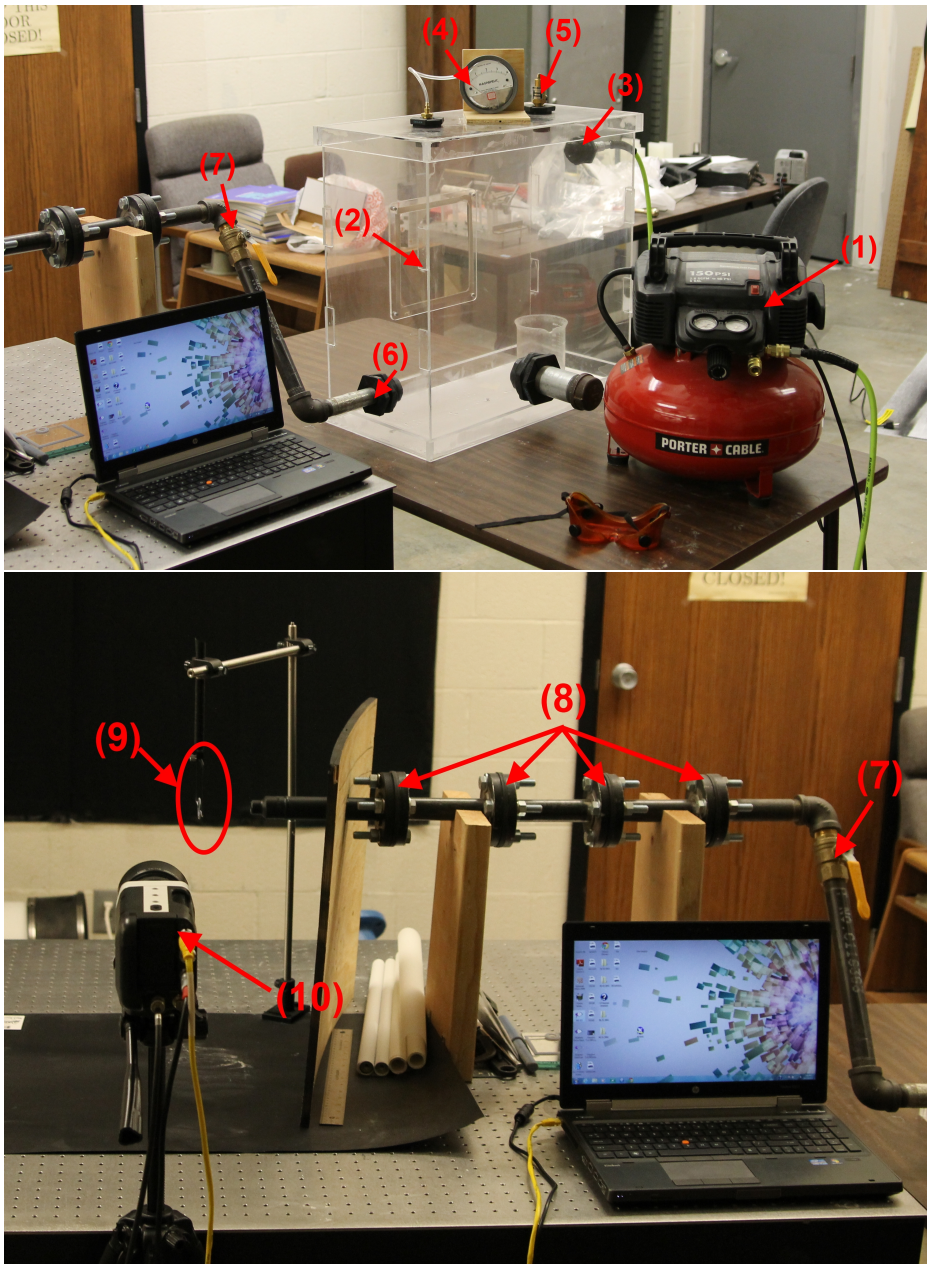

Figure 3.2: Constructed jet apparatus. (1) Compressor, (2) Seeding Chamber, (3) Pressurized air inlet to seeding tank, (4) Low differential pressure gage, (5) Safety valve, (6) Seeding tank outlet, (7) Flow valve, (8) Flanges and meshes, (9) Soap ring, and (10) High-speed Camera

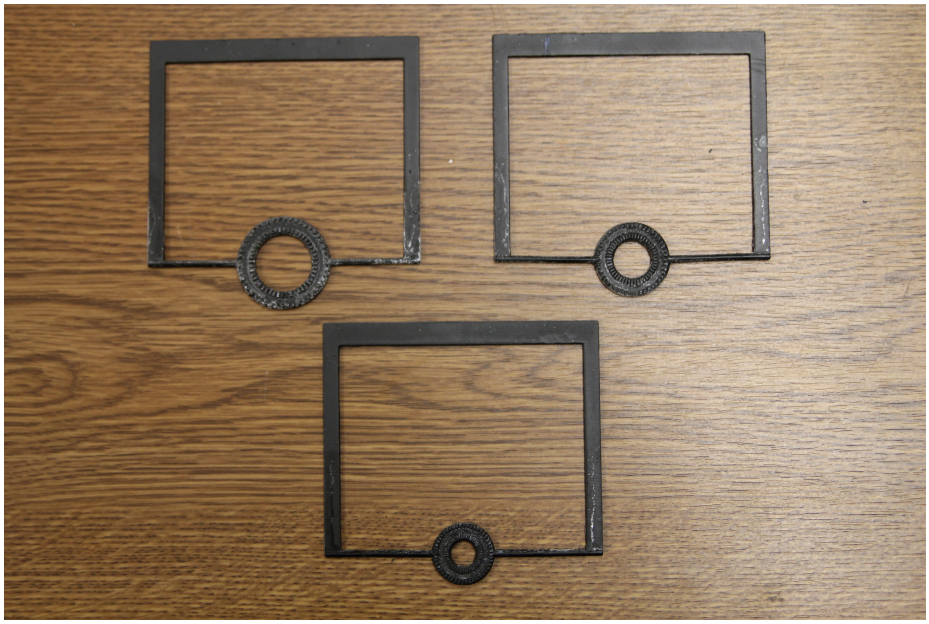

Figure 3.3: Image of the soap rings produced with a 3D printer. The inner diameters are 19.05 mm, 12.7 mm, and 8.38 mm

structed out of acrylic glass so that if particle image velocimetry (PIV) is used, the density of seeded particle can be observed in the chamber prior to any experiments. The seeding chamber has one inlet for the pressurized air, one inlet for the seeding particles, one outlet to pipe, one pressure gage tap, and a safety valve tap as well as a removable window for cleaning and maintenance. Since the pressure is extremely low, a low-differential pressure gage (4 in H_2O Magnehelic, Dwyer Instruments) is selected to read the pressure of the seeding tank. A valve controls the release of the pressurized air in the seeding tank. Three sets of flanges connected by 25.4 mm inner diameter pipe hold the mesh sizes: 10, 20, and 40. The air passes through the 10 mesh first, then the 20, and then the 40. Finally, the air flows through a nozzle that reduces the diameter of the pipe from 25.4 to 6.35 mm.

3.1.5 Soap Ring

The soap rings was designed using computer aided drafting (CAD) software (Solid-Works) and constructed using a 3D printer (Objet 30 PRO, Stratasys). Fig. 3.3

shows the manufactured rings. The rings were designed to be symmetric and so that the jet flow in the cross-sectional plane is minimally affected. Therefore, the stems were placed perpendicular to the cross-sectional plane. At first, the ring was designed to be smoothed so the flow would not be disturbed more than was necessary. This proved problematic since the soap liquid drained off the ring too quickly. The ring is now designed in the fashion of commercial soap rings with tiny fins along the radial direction of the soap rings. This slows the flow of liquid and limits the thinning of the soap film prior to jet initiation. Three inner diameters of the rings were selected: 19.05 mm, 12.7 mm, and 8.38 mm. Optical steel posts and a fixed filter mount were adapted to hold the ring 7.5 cm in front of the nozzle from above. This allows the ring to be dipped into the soap solution by bringing the solution's beaker up to the ring from below. This prevents the ring from shifting positions when the soap film is replaced between experiments.

3.2 Fluid Properties

The soap fluid is characterized by three main properties: the density, the viscosity, and the surface tension. The density and viscosity will be controlled by adding glycerol to distilled H_2O prior to adding the surfactant. In order to vary the surface tension, the surfactant sodium dodecyl sulfate (SDS), $C_{12}H_{25}NaO_4S$, was selected [22–24].

3.2.1 Specific Gravity

In order to calculate the density of the solution, a hydrometer was used, which measures the specific gravity of liquids. A hydrometer is generally a glass bulb that is weighted at the bottom with mercury or other dense materials. When placed in the solution, the bulb will float partly submerged and an inscribed scale provides the specific gravity of the liquid. Due to the fact that additives to a liquid will increase

Figure 3.4: 0.990 to 1.160 Hydrometer

the density of the solution, the density of the soap water is estimated to be in the range of 1.0 to 1.15 g/cm^3. As such, a hydrometer with a scale of 0.990 to 1.160 was selected (ALLA France) (Fig. 3.4).

The procedure to measure the density of the sample is as follows. The solution is placed into a 250 ml cylinder, the hydrometer is then completely submerged into the solution and allowed to come to equilibrium. The specific gravity is read and the process is repeated to get an average specific gravity. The density is calculated using the definition of specific gravity:

$$\text{S.G.} = \frac{\rho}{\rho_{H_2O}} \tag{3.6}$$

where S.G. is the specific gravity of the sample, ρ is the density of the solution, and ρ_{H_2O} is the density of water.

3.2.2 Surface Tension

There are multiple methods to determine the surface tension of a liquid. The three methods considered for this experiment are the du Nouy Method, a stalagmometer, and the capillary tube method. Each method is researched and the advantages and disadvantages are considered. The considerations when choosing the appropriate method are cost, accuracy, and ease of use.

The Du Nouy Method measures the amount of force required to pull a specified

geometry out of a pool of liquid in order to determine the surface tension of the liquid [25]. The advantages of the du Nouy method are that it is considered the most accurate and requires only a small amount of solution; the disadvantage is that it is the more expensive than the alternatives, mainly due to the precision of the geometry needed and the material used for the geometry, platinum [25].

A stalagmometer measures the surface tension of a solution by allowing drops of a reproducible size to slowly form and drop over time. By counting the number of drops that have been produced and measuring the amount of solution used, the volume of each drop can be calculated. This volume is then related to the surface tension via a known liquid's measurements [25]. The advantages of using a stalagmometer is that it is inexpensive and is easy to setup and use. However, the process of one experiment takes about an hour to clean and use. During this hour, the user must focus solely on the experiment since they need to count every droplet. Due to the possibility of missing a drop, as well as the possibility that the droplets may not be a consistent size, this method is considered less accurate than other faster methods of measuring the surface tension [25].

The capillary tube method uses a capillary rise in a small tube to determine the surface tension of the liquid. Due to the surface tension and pressure effects on the liquid, as described by the Young-Laplace equation, a water-based liquid will rise up a small tube (capillary tube). The main advantage of using a capillary tube is that they are most cost effective. The main disadvantage is the accuracy of the tube. The tubes are normally marked with 1 mm increments. It is also sometimes necessary to use a magnifying glass to measure the height [25].

Based on the advantages and disadvantages of each method, as well as the experimental needs, the Capillary Tube Method is the most appropriate. The cost for initial readings and analysis is the most appropriate and the accuracy of the equipment can be adjusted for. It is also easy to use and, as long as caution is taken, the

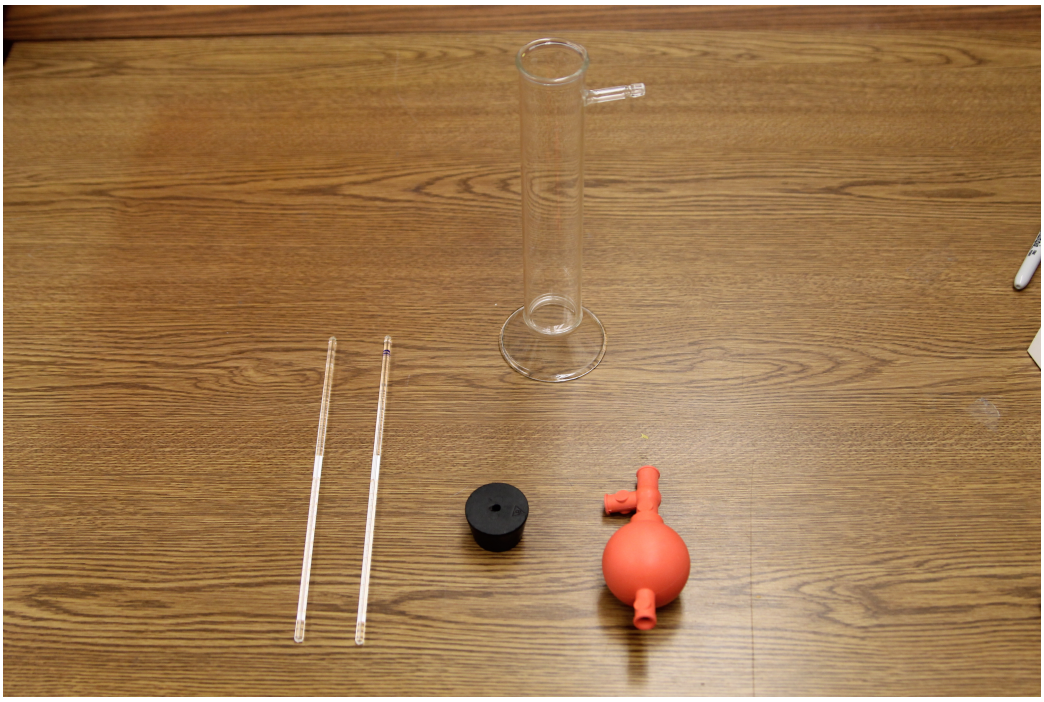

Figure 3.5: Capillary tubes and necessary equipment for measuring surface tension. The capillary tube radii are 0.028 cm.

equipment should be easy to clean. A capillary tube was purchased from Kimble & Chase, shown in Figure 3.5. The capillary tube is cleaned and rinsed with distilled water and 70% ethanol prior and after each measurement. A quantity of sample is placed into the cylinder and the capillary tube with stopper is placed into the cylinder. A rubber bulb is used to expel air through the apparatus until sample comes out of the capillary tube's top. The system is then allowed to come to equilibrium and the height difference is recorded. This is repeated once more. Next, air is withdrawn from the apparatus until the capillary tube is emptied. The system is then allowed to come to equilibrium and the height difference is recorded. This is repeated once more. The surface tension is finally calculated using

$$\sigma = \frac{1}{2} hr\rho \mathrm{g} \tag{3.7}$$

where σ is the surface tension, h is the distance between menisci, r is the radius of

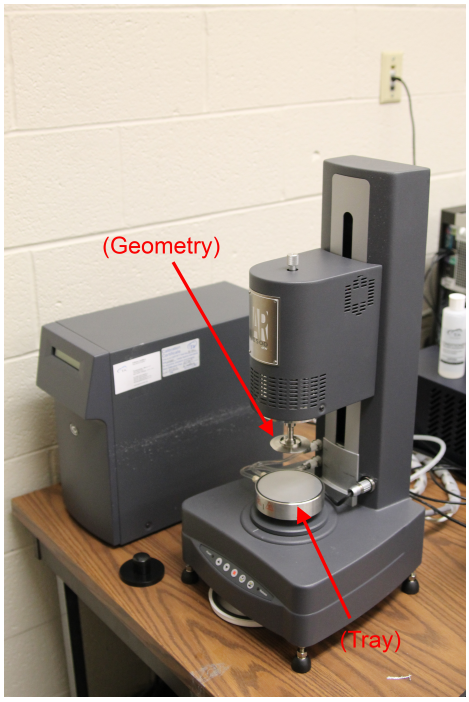

Figure 3.6: AR1500ex Rheometer from TA Instruments.

the capillary, ρ is the density of the sample, and g is the acceleration of gravity. The radius is calibrated using 99% benzene of which the surface tension is known. It was found that the radii of the two capillary tubes used were 0.028 cm.

3.2.3 Viscosity

In order to measure the viscosity, a cone-and-plane type rheometer (AR1500ex, TA Instruments) (Fig. 3.6). The geometry used is a 60 mm diameter 1° Cone with a gap distance of 28 μm. In order to measure the viscosity, 0.984 ml of sample (determined by the geometry) is placed on the tray of the device. The geometry is then lowered to the gap distance from the lower plate. The rheometer is ramped from 0 to 15 Pa of stress; the stress, shear rate, and viscosity are recorded. A viscosity reference standard (Cannon® certified N2) with a viscosity of 1.962 mPa/s at 25°C was used to check the accuracy of the rheometer. The average measured viscosity was 2.418 mPa/s, meaning the rheometer has an error of 23% at this range of geometry. This

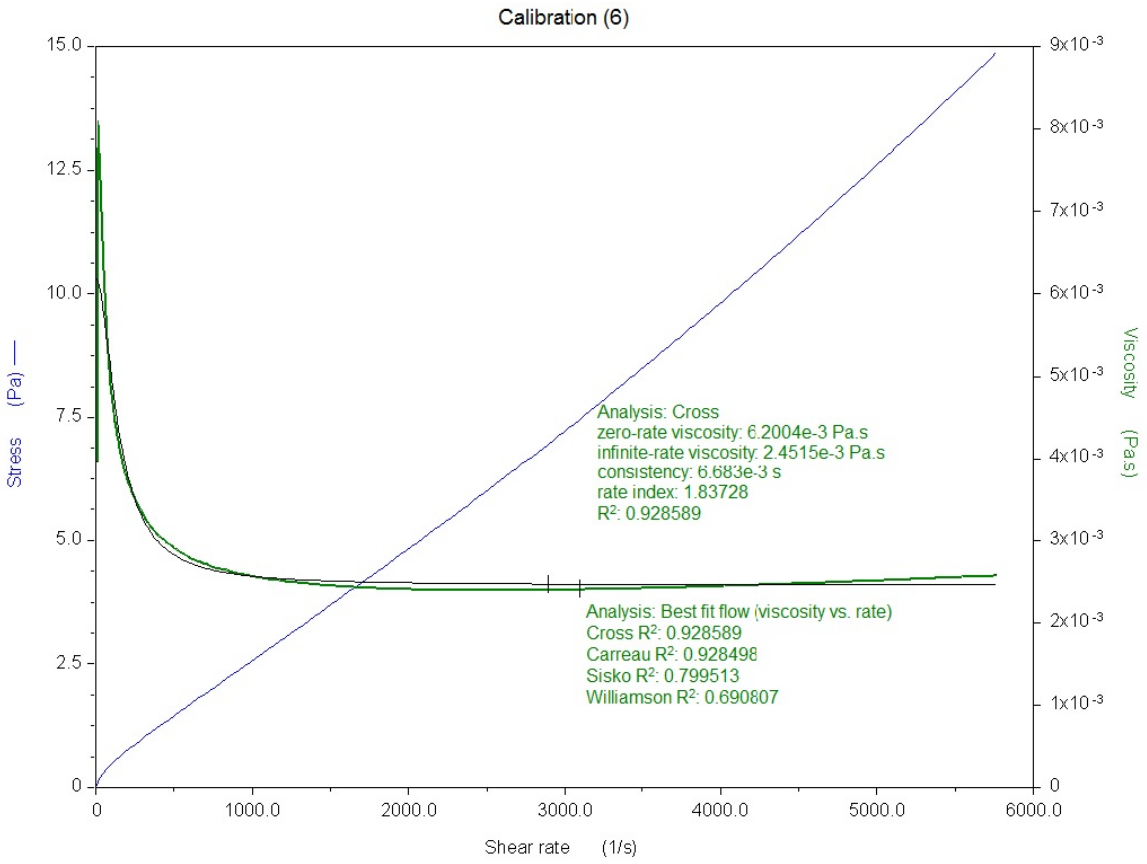

Figure 3.7: Rheometer found viscosity of the Cannon® certified N2 viscosity reference standard at 25°C. True viscosity is 1.962 mPa.s.

is due to the low viscosity of the samples being used. Figure 3.7 shows a resultant graph for the reference standard.

3.2.4 Soap Solution

The decided on soap solution ratio was 5% SDS and 10% glycerol. A range of SDS and glycerol ratios were tested and the 5% SDS/10% glycerol ratio was decided on because it was the most consistent in forming soap bubbles. The surface tension was measured to be 33.8×10^{3} N/m and the density was measured to be 1.022 g/cm^3. The viscosity was determined to be 2.5×10^{-3} Pa.s. Fig. 3.8 shows a resultant graph for the 5% SDS/10% glycerol solution obtained from the rheometer.

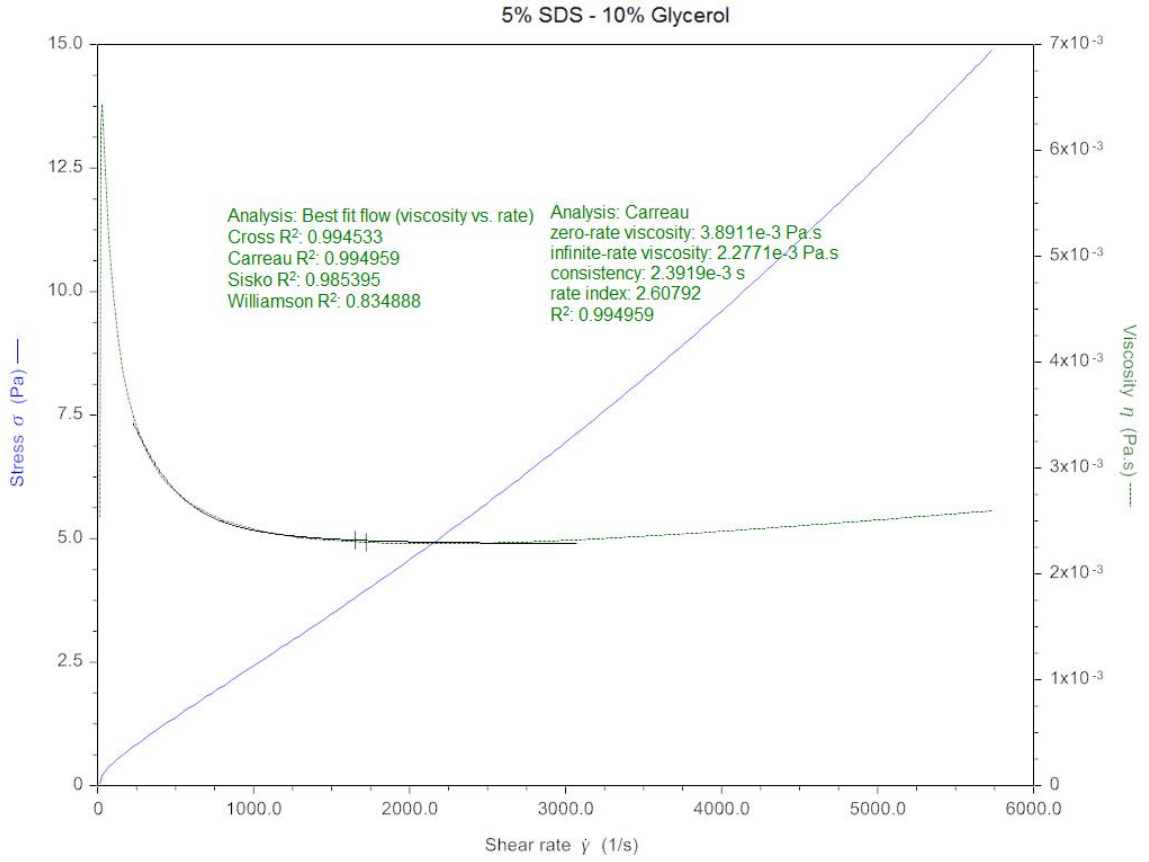

Figure 3.8: Rheometer found viscosity of the 5% SDS/10% glycerol soap solution at 25°C.

3.3 Methods

To study the effect of the fluid flow on the soap bubble formation, high-speed videos of bubbles forming were captured with and without seeding particles. The initial chamber pressure was kept at 0.9 in H_2O and the distance from the nozzle to the soap bubble ring was kept at 75 mm through all experiments to insure accurate results. The images without flow visualization were used to analyze the pinch-off of the bubbles and the images with seeding particles were combined with particle image velocimetry (PIV) to analyze the flow of the jet. A smoke generator (400W Fog Machine, Gemmy Industries Corp) was used to seed the seeding chamber. The density of the particles was controlled for best results. Also, a time difference of 150 μs between the images of an image pair is found to be the optimal time difference. The laser used for PIV (EverGreen 200 mJ, Quantel Laser) has a maximum pulse frequency of 15 hz and the thickness of the laser sheet was measured to be 8 mm. In order to verify the jet flow results, the PIV experiments was performed in steps. First, the jet flow without objects obstructing the flow was analyzed. Next, the jet flow around the soap ring without soap film was examined. Finally, the flow with soap ring and soap film was observed.

Chapter 4

Results and Discussions

4.1 Pinch-off and Minimal Radius of Neck

Figures 4.1, 4.2, and 4.3 illustrate the time series of a soap bubble forming from early formation to the point of first pinch-off for the 19.05 mm, 12.7 mm, and 8.38 mm rings, respectively. The images were captured at 1000 frames per second (fps). When the jet impinges on the soap film, the soap film begins to stretch into a soap tube. At early time, the soap tubes are stable. As the tube expands, a wave-form instability forms. This occurs for the 19.05 mm, the 12.7 mm, and the 8.38 mm rings at 96 ms, 68 ms, and 66 ms, respectively. This instability grows until pinch-off occurs, similar to the instability observed by Plateau and Rayleigh. The total lapse in time from when the jet first impinges on the film to when pinch-off occurs is 154 ms, 108 ms, and 94 ms for the 19.05 mm, the 12.7 mm, and the 8.38 mm rings, respectively.

To analyze the pinch-off, the minimal radius of the tube (r) was compared to the time till pinch-off (τ). For comparison between ring sizes, r was normalized with the radius of the tube at the ring (R) and τ was normalized with the capillary time (τ_c). The capillary time comes from the balance of the inertial forces of the air jet and the

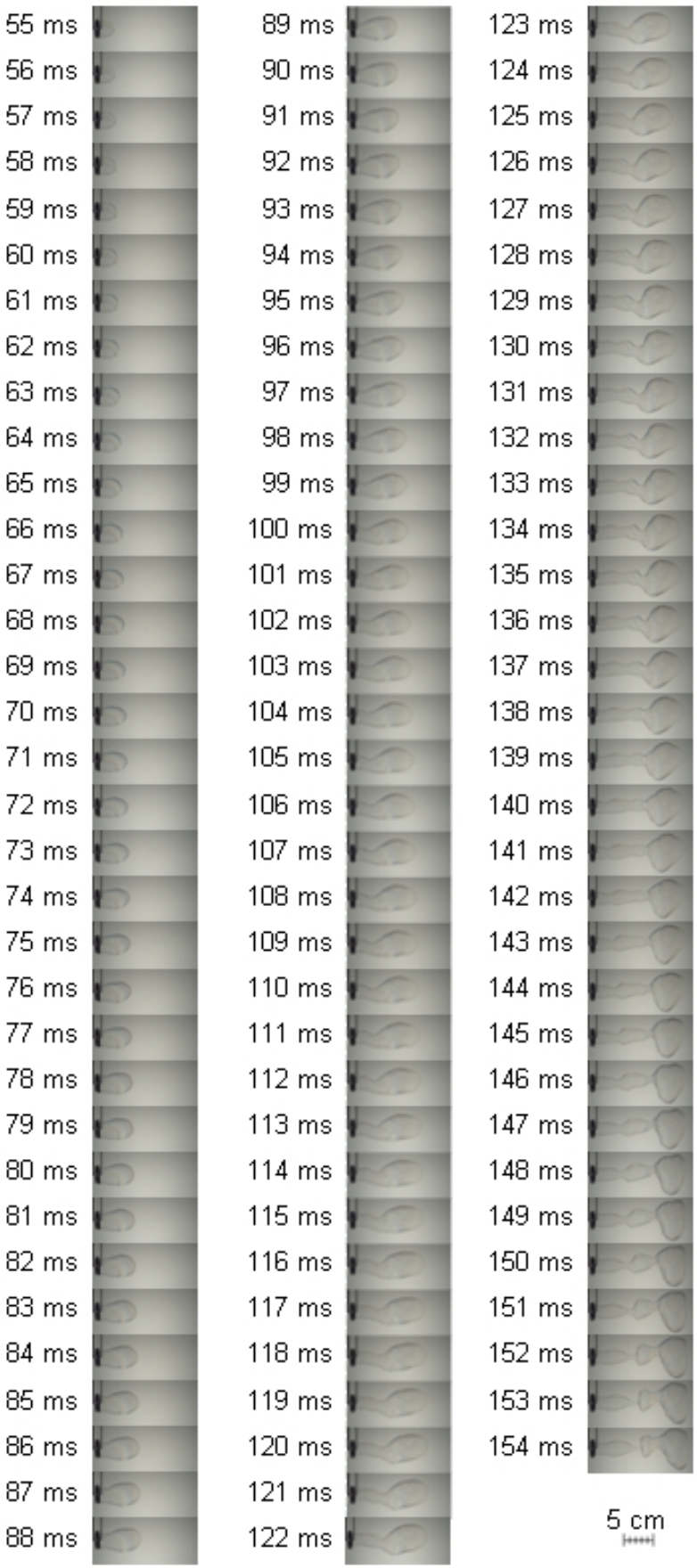

Figure 4.1: Timelapse of bubble formation from near beginning of bubble formation process to pinch-off. Initial pressure of flow is 0.9 in H_2O, ring diameter is 19.05 mm, and distance from nozzle to ring is 7.5 cm. Times are since jet first impinged on soap

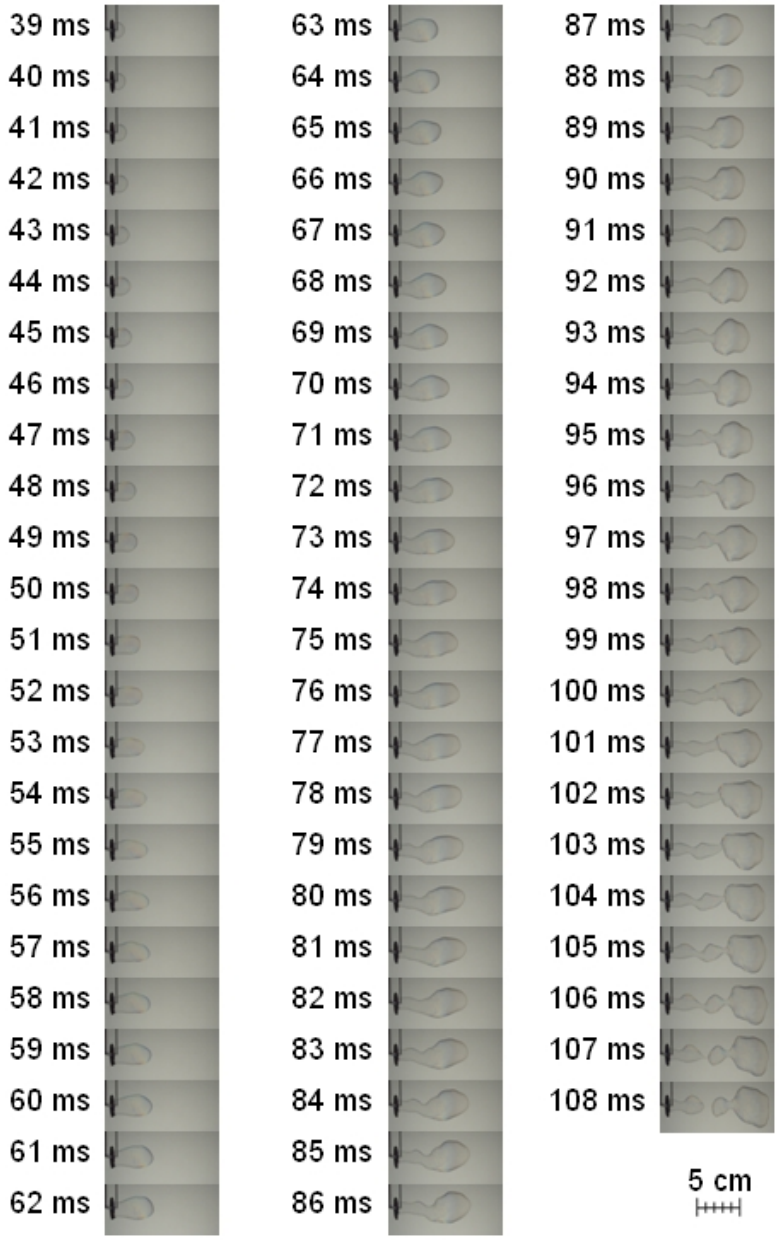

Figure 4.2: Timelapse of bubble formation from near beginning of bubble formation process to pinch-off. Initial pressure of flow is 0.9 in H_2O, ring diameter is 12.7 mm, and distance from nozzle to ring is 7.5 cm. Times are since jet first impinged on soap film.

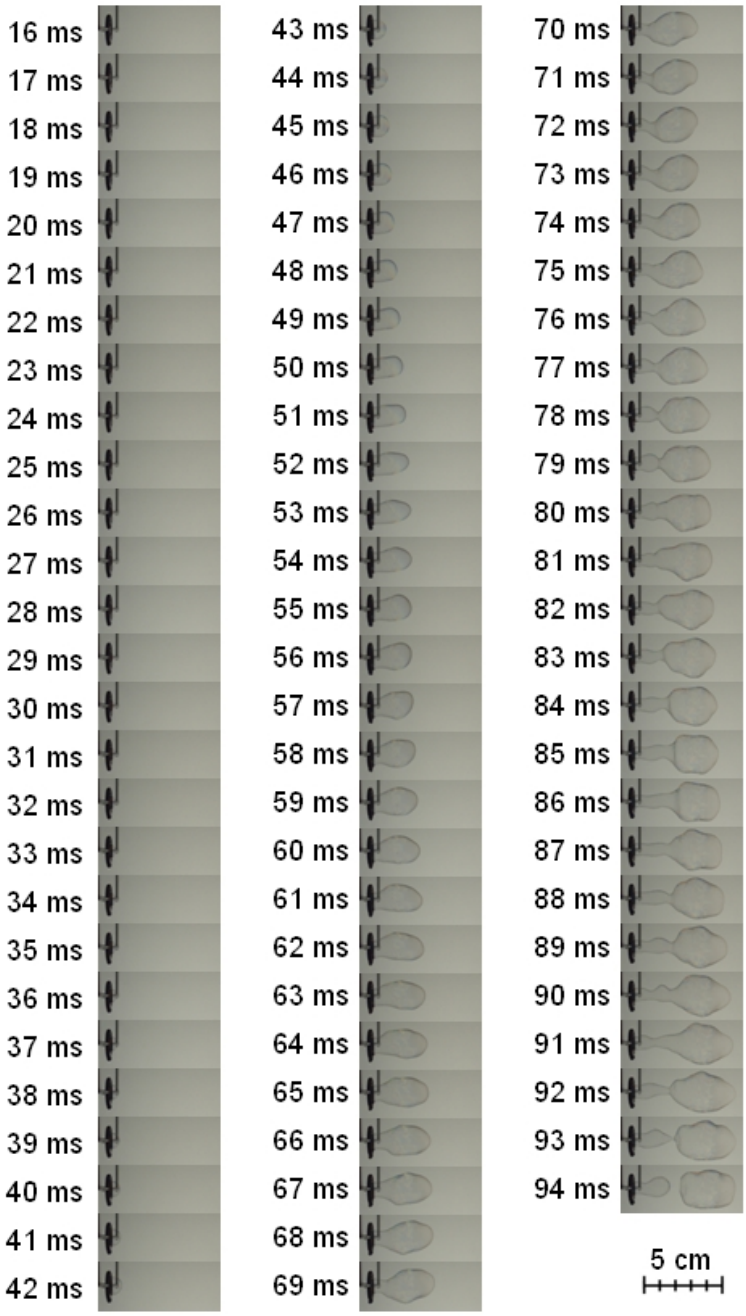

Figure 4.3: Timelapse of bubble formation from near beginning of bubble formation process to pinch-off. Initial pressure of flow is 0.9 in H_2O, ring diameter is 8.38 mm, and distance from nozzle to ring is 7.5 cm. Times are since jet first impinged on soap film.

surface tension of the soap film [26] and is

$$\tau_c = \sqrt{\frac{\rho_g R^3}{\sigma}} \tag{4.1}$$

where ρ_g is the density of the air. The capillary times for the 19.05 mm ring, the 12.7 mm ring, and the 8.38 mm ring is about 6 ms, 3 ms, and 1.5 ms, respectively.

As described in Section 2.8, the minimum radius of the soap tube when approaching pinch-off is proportional to the time left until pinch-off by the power law: $r \propto \tau^{\alpha}$. Normalizing this and taking the logarithm leads to

$$\log \frac{r}{R} \propto \alpha \log \frac{\tau}{\tau_c}. \tag{4.2}$$

Figure 4.4 shows the log plots of normalized radius versus time for each of the rings. As can be seen, the general trend for each of the ring sizes is close to 2/3. In comparison to the results of Gordillo *et al.*, the α for a soap bubble is twice the α for a gaseous thread in liquid. However, it is on the same order as that for the liquid drop in gas. This suggests that the existence of two gas-liquid interfaces may slow the rate of the collapse of the gas flow into liquid until it collapses at the same rate as the liquid flow into gas. It is important to state that the greater α is, the slower the collapse [5]. This is because

$$\frac{dr}{d\tau} \propto \alpha \tau^{\alpha-1}. \tag{4.3}$$

One explanation for this is the two interfaces associated with the soap bubble doubles the pressure difference across the boundary in accordance to Young-Laplace equation. This higher pressure acts against the collapse of the tube, resulting in a slower collapse.

Some differences can be seen between the three ring sizes. The 19.05 mm ring's

(a) 19.05 mm ring

(b) 12.7 mm ring

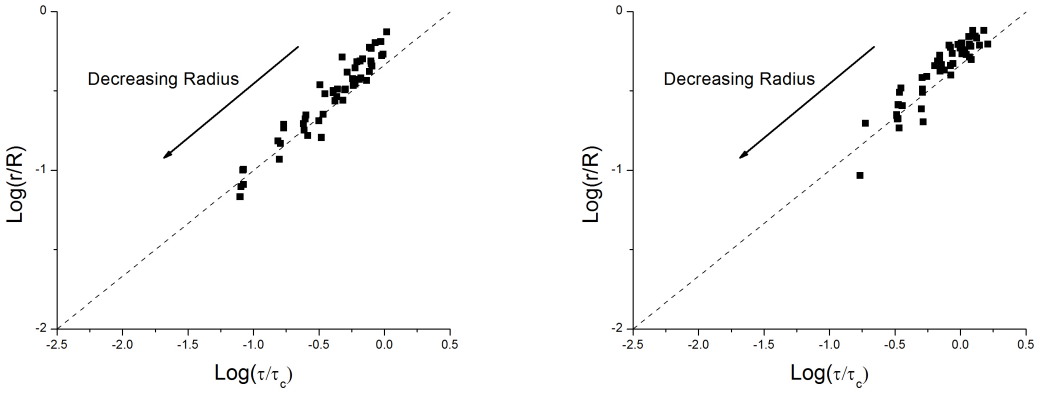

(c) 8.38 mm ring

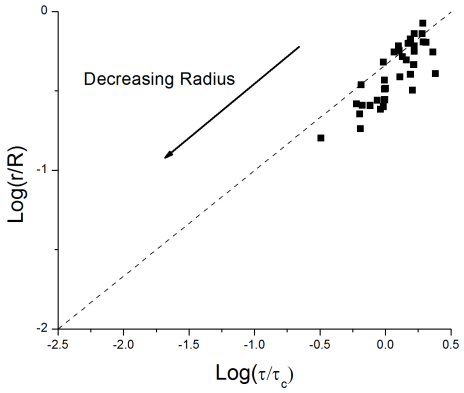

Figure 4.4: Logarithm of the nondimensionalized minimum radius of the soap tube (r/R) as a function of the logarithm of the time until pinch-off nondimensionalized with the capillary time (τ/τ_c) for rings of inner diameter (a) 19.05 mm (51 data points), (b) 12.7 mm (48 data points), and (c) 8.38 mm (37 data points). The dotted line shows the slope of 2/3 for reference.

results shows the smoothest trend. The majority of the data points lie close to the 2/3 slope with a coefficient of determination (R^2) of about 0.92. As the ring becomes smaller, the coefficient of determination decreases. The 12.7 mm ring has a R^2 value of about 0.85 and the 8.38 mm ring has a R^2 value of 0.68. Furthermore, there is a shift of in the x-axis as the ring size decreases. This suggests that the speed of collapse is slightly greater for the smaller rings. These differences could be due to the affects of the flow around the ring. The smaller rings have a smaller percentage of flow going into the tube of the soap film. The remainder of the flow most likely will flow around the ring, creating possible vortices and causing perturbations in the soap film. These perturbations may cause variations in the pinch-off. The flow around the ring may also push the soap tube inwards, causing the collapse to happen faster. This hypothesis was examined with particle image velocimetry (PIV) analysis.

4.2 Particle Image Velocimetry

4.2.1 Jet Flow without Obstructions

Figure 4.6 and 4.6 show the progression of the jet flow. The pictures were taken at the maximum pulse frequency for highest possible resolution. The time between each PIV image is 0.0667 s. The overall lapse in time is 0.2 s, compared to the average time to pinch-off being 0.125 s. Figure 4.6a shows the jet flow at about the time the flow impinges on the soap film. The flow is a laminar flow with two vortices due to the jet mixture with the surrounding air. The next two images show the jet during the development of the soap tube. Some vortices can be seen in the middle of the flow but they die out over time. Pinch-off occurs around the time of Fig. 4.6c. A laser with higher pulse frequency needs to be used to determine if the jet flow is quasi-steady during the development of the bubble. However, Fig. 4.6b and 4.6c show similar flows so a current assumption of steadiness can be made. Fig. 4.6d is after pinch-off when

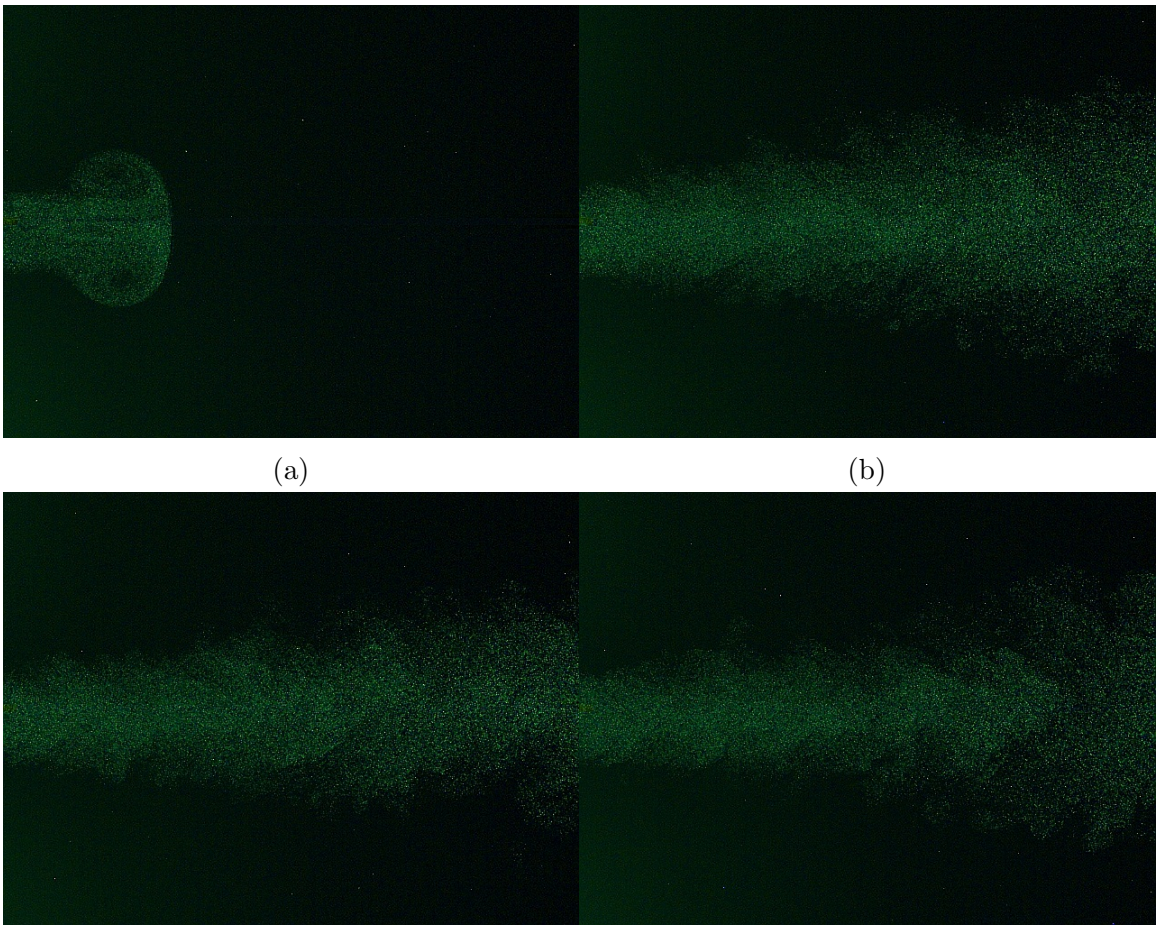

(a) (b)

(c) (d)

Figure 4.5: Progression of jet flow. The sequential images were taken at 15 frames per second. (a) Jet flow at an early time showing the classical jet flow with vortices. (b) Jet flow around peak velocity. (c) Jet flow around time of pinch-off. (d) Jet flow after pinch-off.

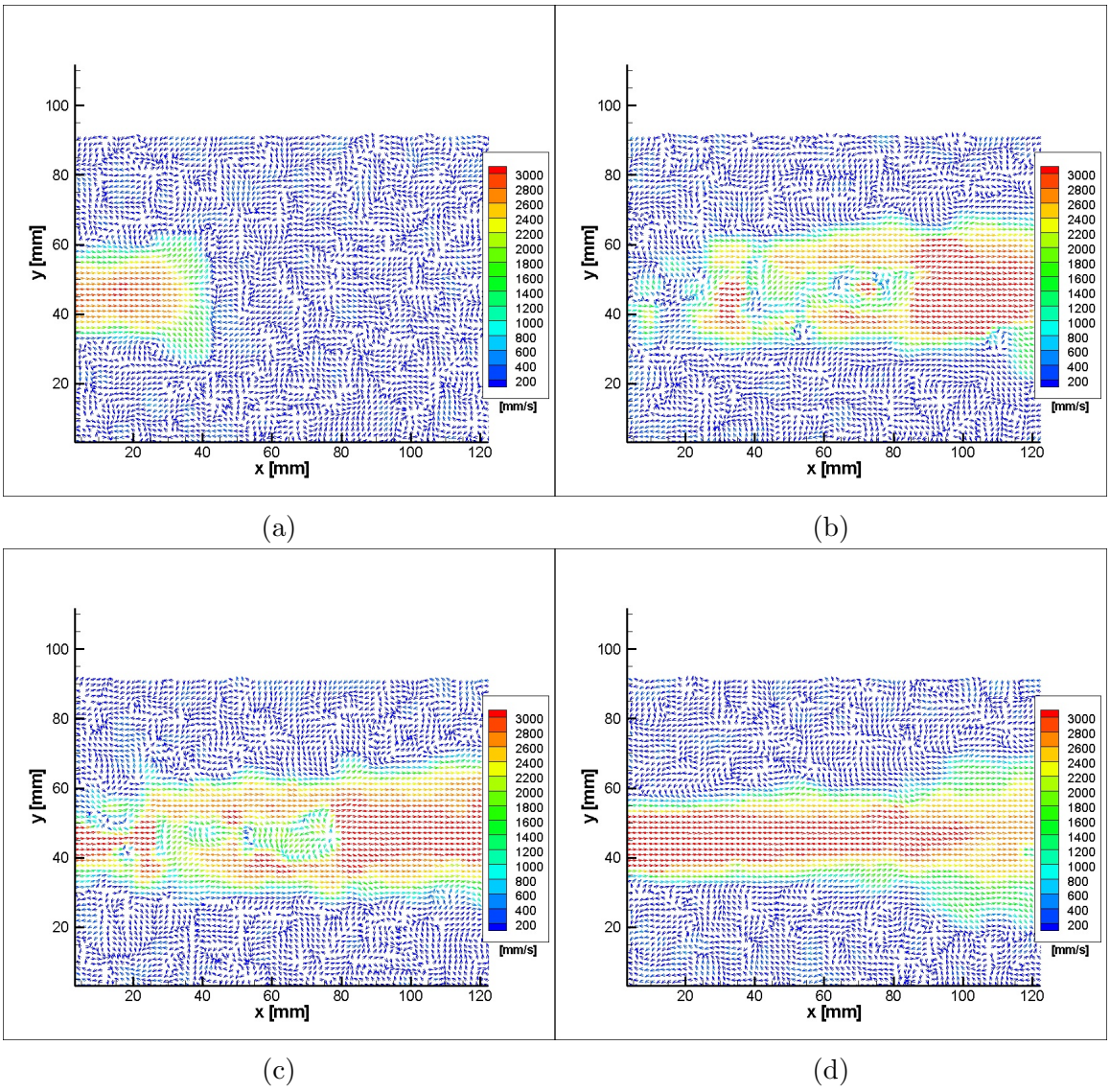

Figure 4.6: Progression of jet flow measured with PIV. The sequential images were taken at 15 frames per second. (a) Jet flow at an early time showing the classical jet flow with vortices. (b) Jet flow around peak velocity showing large amount of vortices near the nozzle (left side of the flow). (c) Jet flow around time of pinch-off displaying slightly less vortices than than previously. (d) Jet flow after pinch-off that has significantly slowed.

the flow has slowed down, showing a laminar flow.

4.2.2 Jet Flow with the Ring

Fig. 4.7 shows the jet flow around the three rings. The outlines of the rings are placed onto the PIV results to show the position of the rings. It can be seen that the 19.05 mm ring (Fig. 4.7a & 4.7b) interferes with the flow the least. A large percentage of the flow passes through the ring. The 12.7 mm ring (Fig. 4.7c & 4.7d) interferes with the flow and only about 50% of the flow passes through the ring undisturbed. The rest of the flow is diverged around the ring and flows off at about 45°. Finally, the 8.38 mm ring (Fig. 4.7e & 4.7f) blocks the flow almost completely. The majority of the flow passes around the ring. However, in contrast to the 12.7 mm ring, the flow around the 8.38 mm ring does not diverge, but continues in the direction of the original flow. The flow that does pass through the 8.38 mm ring is significantly slowed by the flow that passes around the ring.

It should be noted that the flow prior to the soap ring is not as accurate as the flow after the soap ring due to the laser position, which is down stream of the soap ring. This laser position casts shadow around the soap ring, however, a better arrangement could not be constructed at this time. Also, the flow directly surrounding the ring is inaccurate due to the particles leaving or entering the field of view from inside of the soap ring.

4.2.3 Jet Flow with Soap Film

Fig. 4.8 shows the flow interaction with the soap film during early formation of the soap tube. With the presence of the soap film, the flow can no longer pass directly through the ring and at early time, the film acts as a bounding boundary. The flow therefore becomes similar to flow impinging on a circular disk. When the ring or soap film diameter is close to or greater than that of the jet, the flow would take

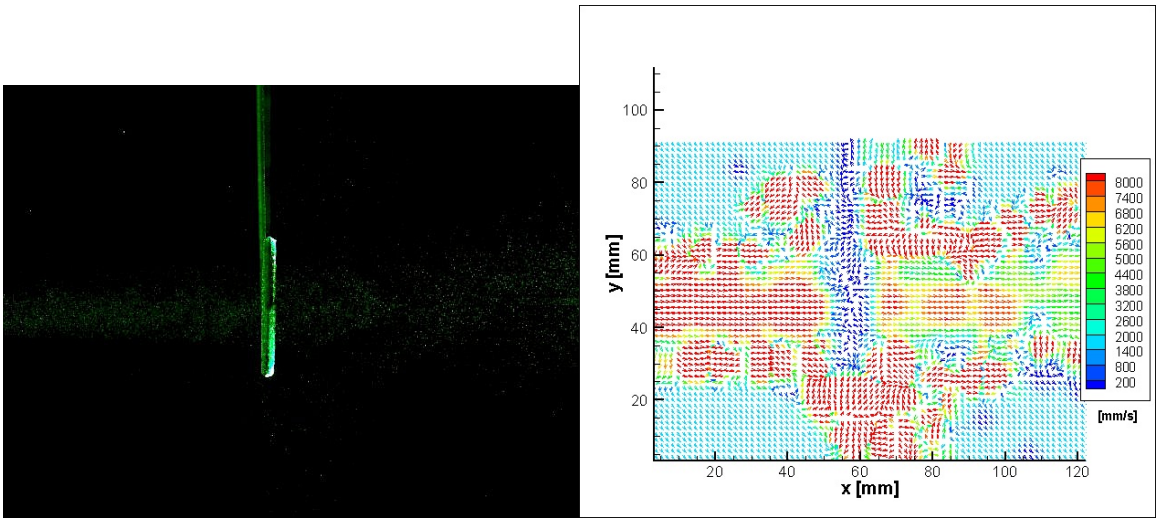

(a) (b)

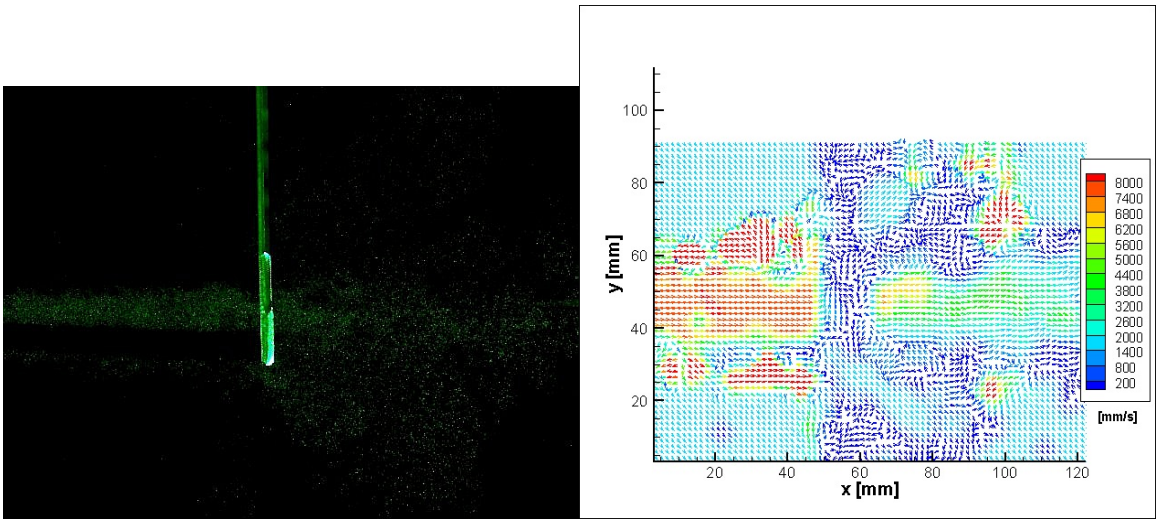

(c) (d)

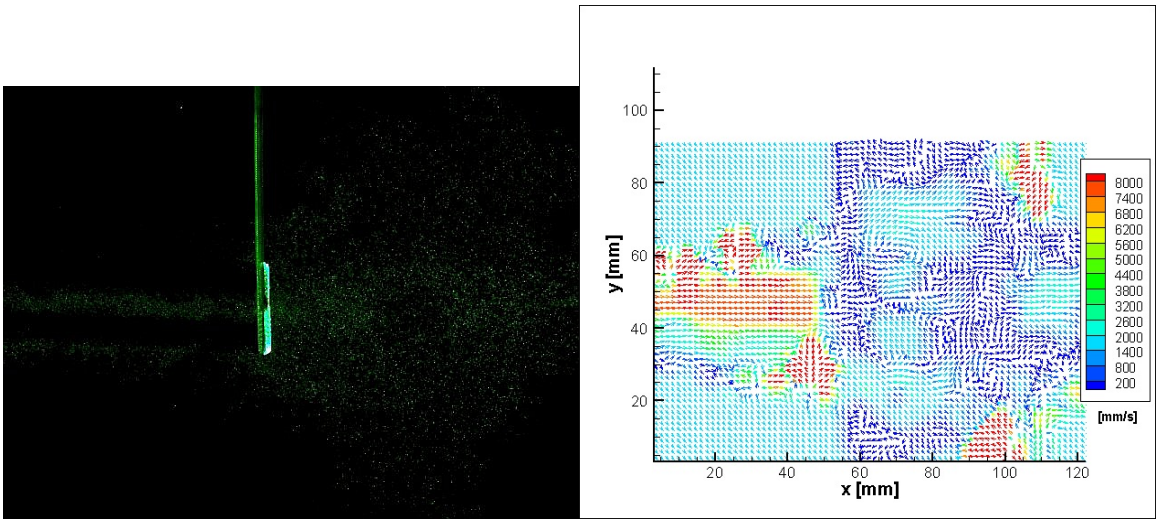

(e) (f)

Figure 4.7: Jet flow around the soap rings. (a & b) Flow around the 19.05 mm ring showing high amount of flow passing through the ring. (c & d) Flow around the 12.7 mm ring showing partial blockage of flow. (e & f) Flow around the 8.38 mm ring showing almost complete blockage of the jet flow.

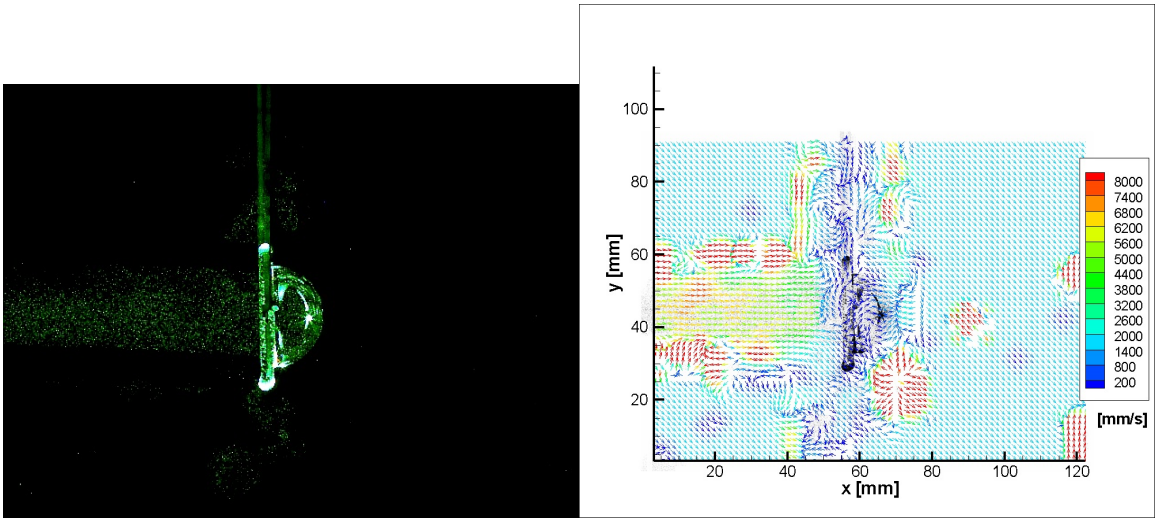

(a) (b)

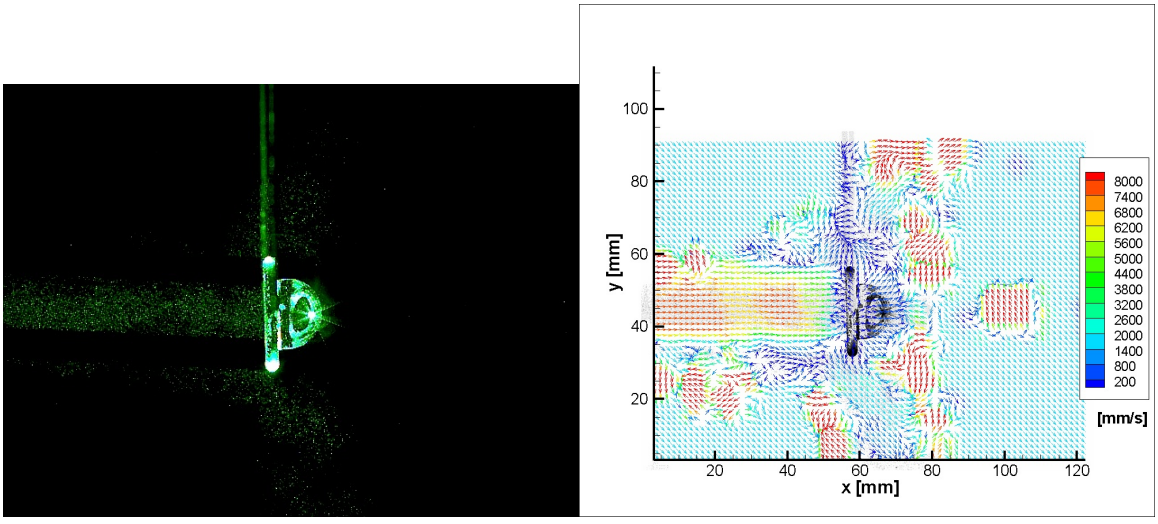

(c) (d)

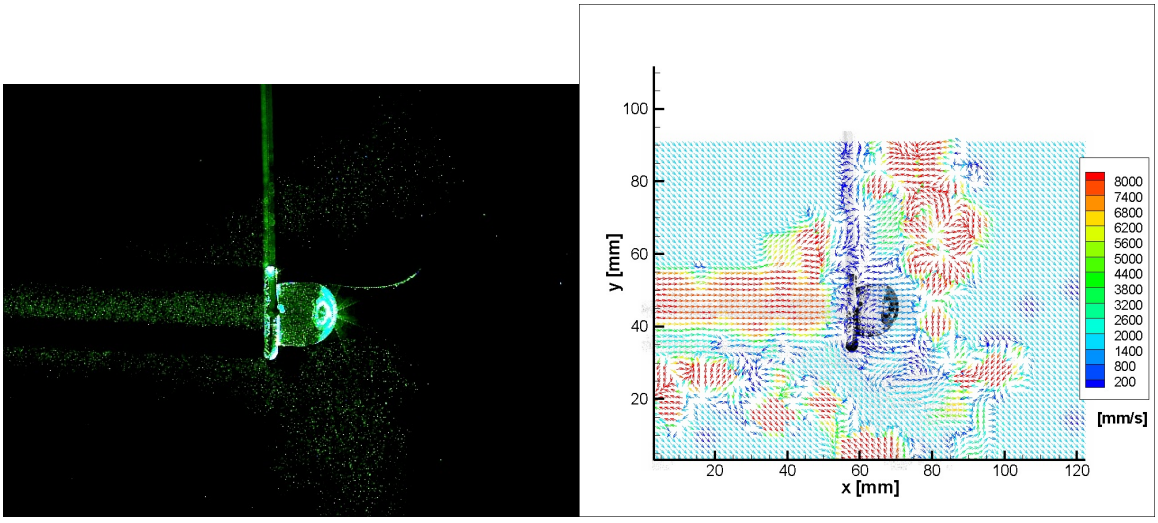

(e) (f)

Figure 4.8: Flow visualization and PIV results of the jet interacting with the soap bubble during early formation for the three ring sizes: (a & b) 19.05 mm, (c & d) 12.7 mm, and (e & f) 8.38 mm

the form of a flow impinging on a flat surface. This would mean that the flow would be directed perpendicular to the original direction of flow. This is the case for the 19.05 mm ring (Fig. 4.8a & 4.8b). The flow acts on the soap film before flowing nearly radially outwards. As the diameter of the ring or soap film decreases, the flow being directed outwards by the soap film will combine with the flow passing around the ring, causing the resultant direction of flow to be less than 90° from the original direction (Fig. 4.8c & 4.8d). When the smallest ring is considered (Fig. 4.8e & 4.8f), the flow almost completely raps around the forming soap tube. It should be noted that patches of flow exist where flow is unexpected due to light being refracted by the soap film. The general trends of the flow are still valid, but the magnitude of the velocities may be altered.

Fig. 4.9 shows the flow interaction with the soap liquid tube later into the formation of the soap bubble. In this example, the flow reaches further towards the front of the soap tube as the diameter of the ring or soap tube decreases. For the 19.05 mm ring (Fig. 4.9a & 4.9b) the flow reaches about half of the length of the soap tube. For the 12.7 mm ring (Fig. 4.9c & 4.9d) the flow reaches nearly to the front of the soap tube. Finally, for the 8.38 mm ring (Fig. 4.9e & 4.9f) the flow reaches in front of the soap tube. This is due to the observed flow differences at early formation of the soap tube.

These flow patterns seem to confirm the hypothesis that the flow that passes around the rings may perturb the soap tube, leading to the variances in the pinch-off. For the 19.05 mm ring, there is little flow on the outside of the soap tube, causing little perturbation so that the pinch-off occurs regularly. The 12.7 mm has a larger amount of flow passing outside of the soap tube and causing more perturbation to the soap tube than the 19.05 mm ring. This leads to more irregularity in the pinch-off. However, the flow outside of the soap tube diverges meaning the amount of perturbations is not as high as is possible. The 8.38 mm ring has the greatest amount

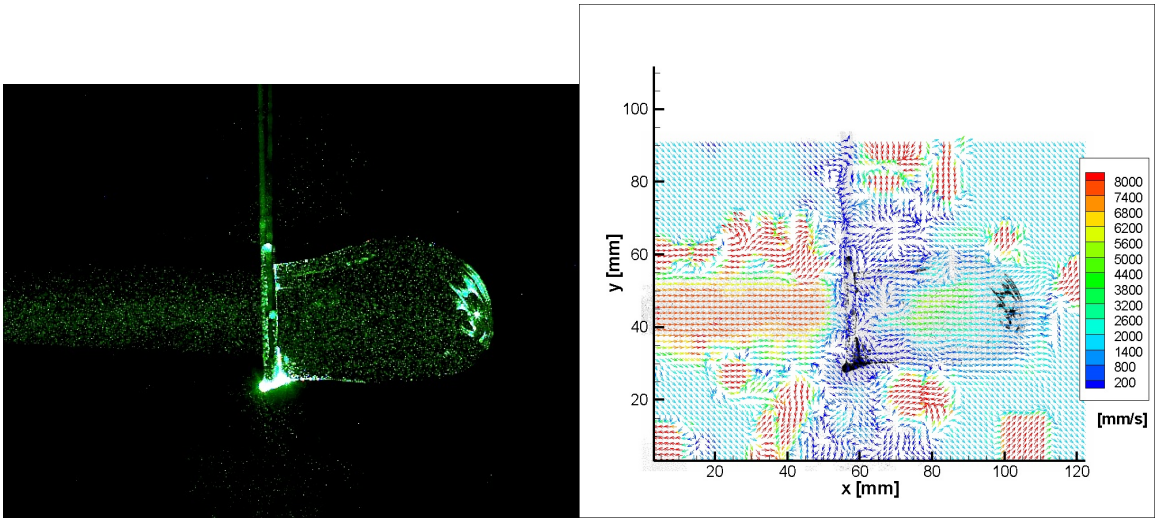

(a) (b)

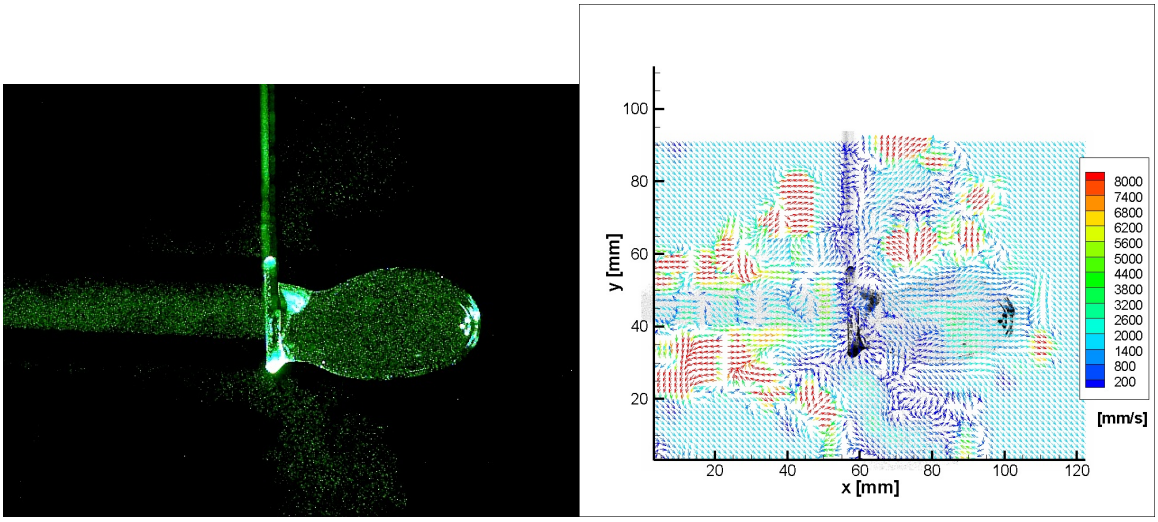

(c) (d)

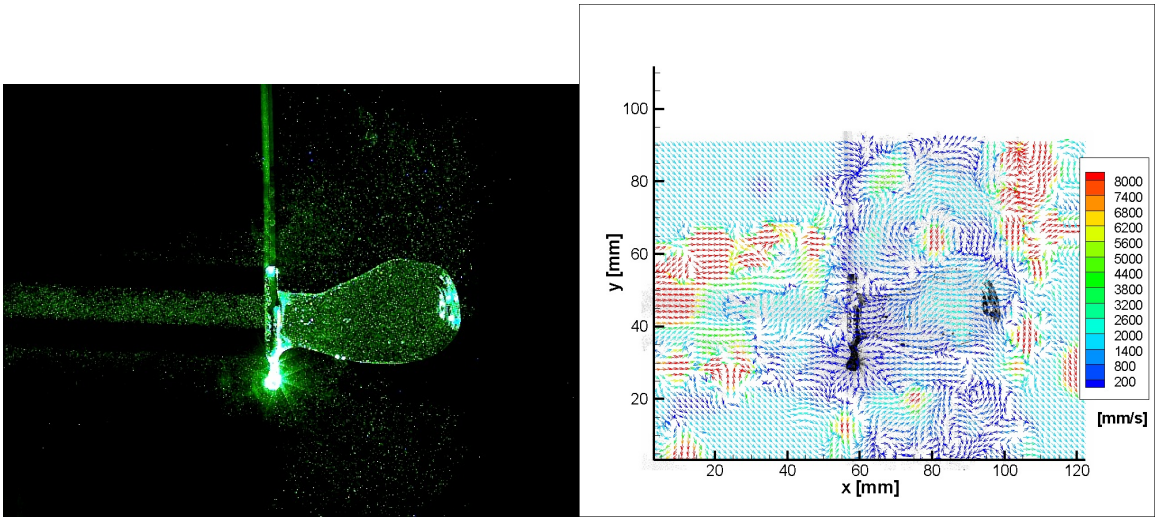

(e) (f)

Figure 4.9: Flow visualization and PIV results of the jet interacting with the soap bubble during later formation for the three ring sizes: (a & b) 19.05 mm, (c & d) 12.7 mm, and (e & f) 8.38 mm

of flow outside of the soap tube, causing the greatest variance.

Chapter 5

Conclusions

Soap bubbles are a common inter-facial fluid dynamics phenomenon that is useful in industries. They can be used to create hollow spheres that are used in light weight material and for ships to reduce the weight while withstanding higher pressures. It can also be used to study the pressure and flow caused by moving wind turbine blades. However, the flow affect on the formation of the soap bubble has been studied relatively little in comparison to similar systems such as gas bubbles in liquid and liquid drops in gas. Therefore, this research aimed to study how the fluid flow and the existence of two gas-liquid interfaces affect the soap bubble formation.

It was found that the minimal radius of the soap tube when approaching the pinch-off follows the power law $r \propto \tau^{\alpha}$ where α is about 2/3. Furthermore, the coefficient of determination decreases as the ring diameter decreases with all other conditions remaining the same. It was shown using particle image velocimetry (PIV) that this is due to the change in flow outside of the soap tube. When the ring is large, little jet flow exists outside of the soap tube. As the ring size decreases, the amount of flow outside the soap tube increases, causing a greater amount of perturbations in the soap tube and increasing the variance in the pinch-off.

5.1 Future Work

This research can continue in multiple directions. One interesting subject would be to see how the soap solution's properties affect the pinch-off by varying the density, viscosity, and surface tension. This could lead to a further relationship for α that is a function of the properties. Also, with the variance of the properties, relationships between the length of the soap tube when pinch-off occurs and how the bubble forms can be examined. Furthermore, the scaling law behavior of the soap bubble can be examined.

Another interesting direction is to see how the flow inside the soap tube affects the pinch-off. Planar laser induced fluorescence (PLIF) can be used to do this. Currently, the refraction and reflection of the laser off of the soap film causes bright spots on the soap film that interfere with the tracking of the seeding particles. PLIF would allow a filter to be used to prevent the capture of the laser light being refracted and reflected allowing only the particles to be observed.

Bibliography

[1] C. V. Boys, *Soap Bubbles: Their Colors and Forces Which Mold Them.* Dover Publications, 1911.

[2] F. Behroozi, "Soap bubbles in paintings," *American Journal of Physics*, vol. 76, pp. 1087–1091, 2008.

[3] A. Prosperetti, "Bubbles," *Physics of Fluids*, vol. 16, pp. 1852–1865, 2004.

[4] H. Wijshoff, "The dynamics of the piezo inkjet printhead operation," *Physics Reports*, vol. 491, pp. 77–177, 2010.

[5] W. Hoeve, B. Dollet, M. Versluis, and D. Lohse, "Microbubble formation and pinch-off scaling exponent in flow-focusing devices," *Phys. Fluids*, vol. 23, 2011.

[6] "Droplet formation," tech. rep., Department of Chemical Engineering and Biotechnology, University of Cambridge, 2013.

[7] P. Garstecki, M. J. Fuerstman, H. A. Stone, and G. M. Whitesides, "Formation of droplets and bubbles in a microfluidic t-junction – scaling and mechanism of break-up," *Royal Society of Chemistry*, 2006.

[8] "Whatever floats your boat," tech. rep., College of Engineering and Science, Clemson University, 1999.

[9] R. Erickson, "Foams on the cutting edge," tech. rep., The American Societyl of Mechanical Engineers, 1999.

[10] "Wind turbine interactions with birds, bats, and their habitats: A summary of research results and priority questions," tech. rep., National Wind Coordinating Collaborative, 2010.

[11] C. Isenberg, *The Science of Soap Films and Soap Bubbles*. New York: Dover Publications, Inc., 1992.

[12] M. C. Potter, D. C. Wiggert, and B. H. Ramadan, *Mechanics of Fluids*. CL Engineering, 2012.

[13] P. Gennes, F. Brochard-Wyart, and D. Quéré, *Capillarity and Wetting Phenomena: Drops, Bubbles, Pearls, Waves*. New York: Springer-Verlag New York, Inc., 2004.

[14] J. Plateau, *Experimental and Theoretical Statics of Liquids Subject to Molecular Forces Only*. Gauthier-Villars year =.

[15] B. Lautrup, *Physics of Continuous Matter: Exotic and Everyday Phenomena in the Macroscopic World*. London: IOP Publishing, 2005.

[16] S. Ramakrishnan, R. Kumar, and N. R. Kuloor, "Studies in bubble formation - i: Bubble formation under constant flow conditions," *Chemical Engineering Science*, vol. 24, pp. 731–747, 1969.

[17] J. C. Burton, R. Waldrep, and P. Taborek, "Scaling and instabilities in bubble pinch-off," *Physics Review Letters*, vol. 94, 2005.

[18] S. T. Thoroddsen, T. G. Etoh, and K. Takehara, "Experiments on bubble pinch-off," *Phys. Fluids*, vol. 19, 2007.

[19] J. M. Gordillo, A. Sevilla, J. Rodríguez-Rodríguez, and C. Martínez-Bazán, "Axisymmetric bubble pinch-off at high reynolds numbers," *Phys. Rev. Lett.*, vol. 95, 2005.

[20] E. Breatnach, G. C. Abbott, and R. G. Fraser, "Dimensions of the normal human trachea," *AJR*, vol. 142, pp. 903–906, May 1984.

[21] J. Groth and A. V. Johansson, "Turbulence reduction by screens," *J. Fluid Mech.*, vol. 197, pp. 139–155, 1988.

[22] "Sodium lauryl sulfate," Tech. Rep. 151-21-3, Department of Health and Ageing, NICNAS, Australian Government, October 2007.

[23] *European Pharmacopoeia 5.0.* Europe: Council of Europe, 2005.

[24] X. Bai and J. Liu, "Bubble based micro/nano fabrication method," *Micro Nano China*, pp. 10–13, 2007.

[25] J. Hill, "Conducting surface tension measurements for compliance with chromium mact," tech. rep., Scientific Control Laboratories, 1995.

[26] W. Hoeve, S. Gekle, J. H. Snoeijer, M. Verseluis, M. P. Brenner, and D. Lohse, "Breakup of diminutive rayleigh jets," *Phys. Fluids*, vol. 22, 2010.

Appendices

Appendix A

List of Materials

List of parts

Part Name	# of Parts	Supply Company	Part #
Ring Mount:			
12 in. Stainless Steel Post	3	Edmund Optics	83-150
6 in. Stainless Steel Post	1	Edmund Optics	83-147
Post Holder and Sliding Base Plate	1	Edmund Optics	59-006
Fixed Filter Mount	1	Edmund Optics	54-996
Right Angle Post Clamps	2	Edmund Optics	53-357
Jet Nozzle:			

1 in. x 6 in. Unthreaded Pipe	3	McMaster-Carr	1120T54
1 in. x 6 in. Threaded-on-One-End Pipe	1	Mcmaster-Carr	7753K156
1 in. Pipe Slip-on-Flange	8	McMaster-Carr	68095K132
Rubber Gasket	8	McMaster-Carr	9473K81
1/2 in. - 13 Bolt, 3 in. Length	16	McMaster-Carr	92865A724
1/2 in. - 13 Hex Nuts	16	McMaster-Carr	95462A033
1/2 in. Lock Washers	16	McMaster-Carr	92147A033
1/2 in. Washers	16	McMaster-Carr	90126A033

Pressure and Seeding Tanks:

Banjo Bulkhead Tank Fitting, 1/2 in.	3	Kelly Supply Co.	TF050
Banjo Bulkhead Tank Fitting, 1 in.	1	Kelly Supply Co.	TF100
Banjo Bulkhead Tank Fitting, 2 in.	1	Kelly Supply Co.	TF200